



Synthesis of CuO nanoparticles for catalytic application via ultrasound-assisted ball milling

Bing Yang, Ding Chen*

College of Materials Science and Engineering, Hunan University, Changsha 410082, P. R. China

Received 20 October 2016; Received in revised form 12 February 2017; Accepted 23 February 2017

Abstract

In this study, copper oxide (CuO) nanoparticles were successfully prepared by ultrasound-assisted ball milling at a low temperature using $\text{Cu}(\text{CH}_3\text{COO})_2$ as raw material. The as-prepared CuO nanocrystals were characterized by X-ray diffraction, transmission electron microscopy, UV-visible spectrophotometer and fluorescence measurements. The results confirmed that the obtained product was single phase CuO with the average particle size of about 20 nm. The catalytic activity of the sample was testified by quantifying the degradation of the methylene blue and rhodamine B aqueous solutions with the assistance of H_2O_2 . The experiments showed that the catalytic performance of CuO, i.e. degradation of methylene blue and rhodamine B aqueous solutions, reached 100% and 98% within 25 min, respectively. In addition, the results of the relative content of $\cdot\text{OH}$ radicals in the aqueous solution proved that the coupling of ultrasound and ball milling remarkably accelerated the chemical reaction.

Keywords: nanopowders, ultrasound, milling, catalytic properties

I. Introduction

In recent years, scientists have become more and more interested in nano-sized oxides of transition metals due to their superior physical and chemical properties quite different from those of their bulk counterparts [1–3]. Copper oxide (CuO) is an important p-type semiconductor with a narrow band gap varying between 1.2 and 1.8 eV [4]. Due to its unconventional band structure, it has a wide range of applications in many areas. For example, CuO has been widely applied in thermal conductivity materials [5], lithium-ion electrode materials [6,7], optoelectronic device systems [8], glucose sensors [9], gas sensing [10], CO oxidation [11], eradication of multi-drug resistant bacteria [12], magnetic storage media [13], solar energy conversion [14], electronics [15] and a crucial component in high temperature superconductors [16], photocatalysts [17] etc. Moreover, CuO with its non-toxicity and low cost is extensively used as a catalyst for oxidative degradation of organic water pollutants [18–20].

In the past thirty years, a wide variety of methods have been employed for synthesis of nano-sized CuO,

such as hydrothermal [21], solvothermal [22], chemical precipitation [23], sol-gel method [24], microwave-assisted [25] and combustion synthesis [26]. However, a simple, low-temperature and environmentally friendly way to prepare nanostructured CuO has rarely been reported.

In this work, we directly synthesized single-phase CuO nanoparticles at low temperature via ultrasound wave-assisted ball milling. We have already prepared ferrite powder and other metal oxide nanoparticles by this approach [27–29]. In addition, we studied the good catalytic properties of the as-prepared CuO nanoparticles by means of decomposing methylene blue and rhodamine B aqueous solutions in the presence of H_2O_2 .

II. Experimental

2.1. Synthesis of CuO

All chemical reagents were analytical-grade used without further purification. Cupric acetate ($\text{Cu}(\text{CH}_3\text{COO})_2$), methylene blue (MB), rhodamine B (RB), H_2O_2 (30%), terephthalic acid (TPA), sodium hydroxide (NaOH), potassium dihydrogen phosphate (KH_2PO_4) were all purchased from Aladdin Ltd. (Shanghai, China). The experiments were carried out

*Corresponding author: tel/fax: +86 731 88821610, e-mail: chending@hnu.edu.cn

in an ultrasonic wave-assisted ball milling device designed by the authors [27]. 20 g of cupric acetate ($\text{Cu}(\text{CH}_3\text{COO})_2$) was used as the raw material and the reaction medium was deionized water (1000 ml). Mass ratio of raw material to milling balls (2 kg, stainless steel balls of 2 mm in diameter) was 1 : 100. The frequency of the ultrasound wave was 40 kHz. The stirring speed was constant at 256 r/min and the experiment temperature in the milling pot was kept below 100 °C. After a certain time interval, the as-milled products were taken out, filtered, and dried for about 24 h at 50 °C. In order to demonstrate the coupling effect of ultrasound-assisted ball milling, ball milling without ultrasound and ultrasound treatment without ball milling were performed respectively on the same device.

2.2. Characterization

X-ray diffraction (XRD, D-5000 Siemens, $\text{Cu K}\alpha$, $\lambda = 0.15418 \text{ nm}$, 2θ rang 20–80°) was used to confirm crystal structure and phase purity of the as-prepared sample. Transmission electron microscopy (TEM, JEOL-1230) was used to observe the average powder particle size and surface morphology. The fluorescence intensities of samples processed by three different approaches were detected by a FL-2500 fluorescence spectrometer with a scan rate of 300 nm/min at the room temperature. Terephthalic acid, NaOH and potassium dihydrogen phosphate of analytical grade were used as a buffer solution. The catalytic activities of the prepared CuO nanoparticles were analysed by using UV-visible spectrophotometer (UV-6000PC).

2.3. Catalytic tests

The obtained CuO nanoparticles were used as catalyst for the oxidation of methylene blue and rhodamine B dye with the assistance of H_2O_2 . The concentration of methylene blue and rhodamine B aqueous solution were all 100 mg/l. 10 mg of the as-prepared powders were dispersed in a 250 ml glass flask containing above

mentioned methylene blue and rhodamine B aqueous solutions, respectively. Then 15 ml of H_2O_2 (30 wt.%) was added to 100 ml aqueous solution of dye in the glass flask which was transferred into the 65 °C bath with continuous stirring for 25 minutes. 5 ml of the mixture was removed every 5 minutes and centrifuged to separate the powders, then diluted with distilled water to 50 ml. The solution concentration was analysed by using UV-visible spectrophotometer (UV-6000PC) at maximum absorbance wavelengths of 664 nm and 554 nm for methylene blue and rhodamine B, respectively. Finally, the degradation efficiency (DE) of the aqueous solution by catalysed oxidation with H_2O_2 was calculated using Eq. 1:

$$DE = \frac{C_0 - C}{C_0} \cdot 100 \quad (1)$$

where C_0 and C are concentrations of the dye solution before and after reaction, respectively.

III. Results and discussion

3.1. Structural characterization

Figure 1 shows the XRD patterns of $\text{Cu}(\text{CH}_3\text{COO})_2$ milled for different time by using aqueous ball milling with ultrasonic wave, which clearly reveals the evolution of raw materials during the processing. The results show that $\text{Cu}(\text{OH})_2$ phase starts to form in the first 6 h, which is marked with the white rhombus pattern. With the reaction continuing, the starting raw materials almost disappeared and the amount of $\text{Cu}(\text{OH})_2$ increased. At the same time, the diffraction peaks of CuO gradually appeared when the ball milling time was extended to 12 h. Based on the principle of mechanochemistry [30], the continuous collision and abrasion by stainless steel balls can induce the decomposition reactions of $\text{Cu}(\text{OH})_2$. Moreover, the ultrasonic waves are able to substantially reduce the onset temperature of the decomposition. Generally, the cavitations caused by the

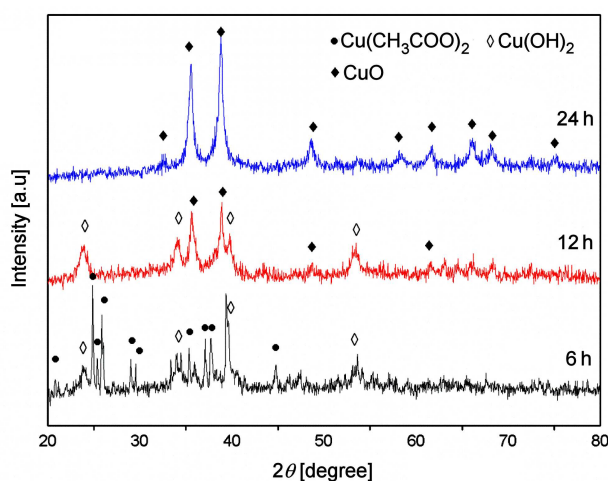


Figure 1. XRD patterns of reaction products prepared by ultrasound-assisted ball milling after different time

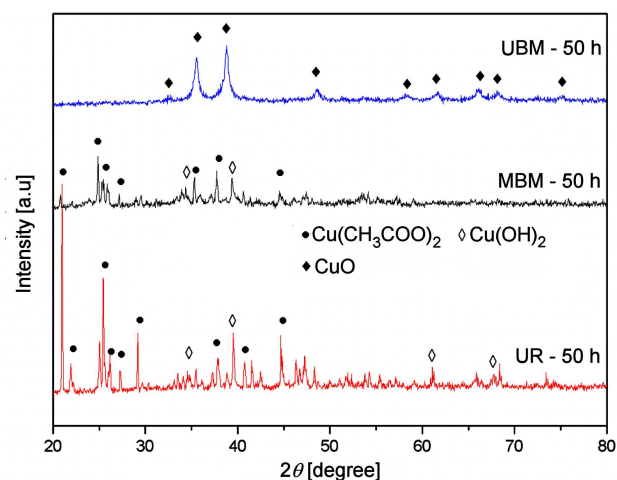


Figure 2. XRD patterns of reaction products prepared by: ultrasound radiation (UR), mechanical ball milling (MBM) and ultrasound-assisted ball milling (UBM)

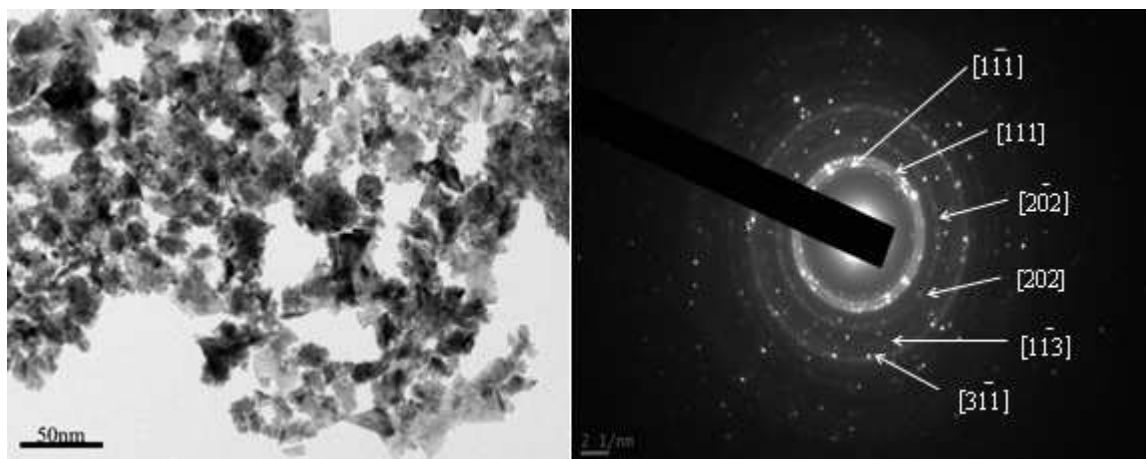


Figure 3. TEM image (a) and SAED pattern (b) of as-synthesized CuO nanoparticles by ultrasound-assisted ball milling

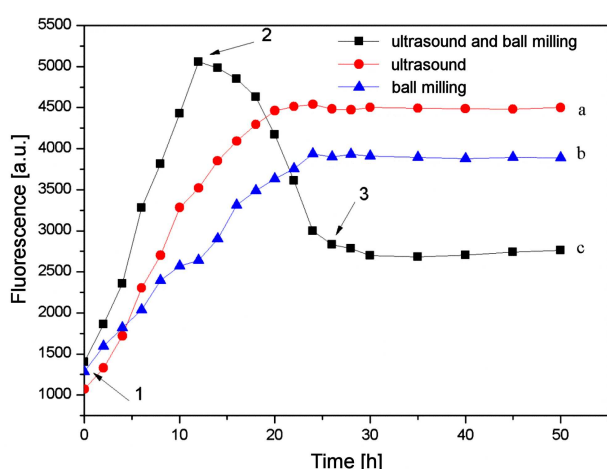


Figure 4. Change of fluorescence intensity as a function of processing time using three different synthesis approaches

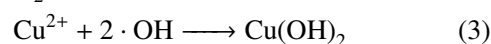
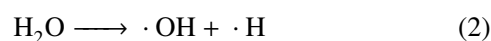
chemical and mechanical effects of ultrasound can result in the formation, growth and implosive collapse of bubbles in a liquid [31]. After milling for 24 h, single phase CuO with a well-developed XRD pattern is obtained, indicating that $\text{Cu}(\text{OH})_2$ has completely been decomposed into CuO.

For comparison, the two approaches of ball milling without ultrasound assistance and ultrasound assistance without ball milling were studied. According to Fig. 2 it can be seen that no CuO phase is formed by these two approaches after 50 h. The result demonstrates the coupling effect of ultrasound assisted ball milling. TEM image and selected area electron diffraction (SAED) pattern of the as-milled CuO nanoparticles for 50 h are shown in Fig. 3. It is observed that the well dispersed particles exhibit regular and uniform morphology. The average size of CuO particles is around 20 nm.

3.2. Spectroscopy – evaluation of $\cdot\text{OH}$ radicals

The concentration of $\cdot\text{OH}$ radicals after different reaction time can be used as the basis for studying the coupling effect of ultrasound radiation and ball milling. The fluorescence intensity of the solution can be used to quantitatively measure free-radical species by introduc-

ing radical-sensitive fluorescence indicators, demonstrating the number of hydroxyl radicals generated in the system [32]. The stronger the fluorescence intensity, the more hydroxyl radicals are generated. As shown in Fig. 4, three curves of fluorescence intensity rise rapidly during 0–10 h with a large number of $\cdot\text{OH}$ radicals quickly generated. However, it was observed clearly that the fluorescence intensity in the solution of the ultrasound assisted ball milling raised faster than that of ball milling or ultrasound radiation only, demonstrating that the presence of a coupling effect of ultrasound and mechanical forces provides more reaction activation energy for chemical reaction. After that, the fluorescence intensity decreased in ultrasound assisted ball milling due to the formation of CuO. The corresponding chemical reaction equations are listed as follows:



Therefore, it is necessary to consume a large amount of $\cdot\text{OH}$ for generating CuO. In addition, it is clearly shown that at the time when fluorescence intensity starts to drop (Fig. 4, arrow 2 on curve c), CuO begins to emerge as confirmed by XRD data. Eventually, when the reaction completes (Fig. 4, near arrow 3 on curve c), the fluorescence intensity reaches a plateau and the reaction system is in a state of equilibrium. However, fluorescence intensity curve of ultrasound radiation or ball milling only has shown an increasing trend until the system reached equilibrium. According to the above observations, it can be concluded that the coupling effect of ultrasound radiation and ball milling produces a lot of $\cdot\text{OH}$, which plays an important role in the synthesis of CuO nanoparticles.

3.3. Catalytic properties

The excellent catalytic activity of the synthesized CuO nanoparticles was illustrated by its degradation of methylene blue and rhodamine B aqueous solution

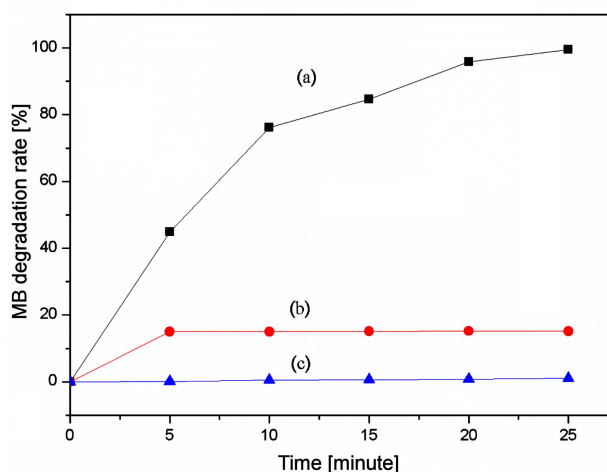


Figure 5. Time profiles of MB degradation rate:
a) MB + H₂O₂ + CuO nanoparticles, b) MB + H₂O₂
and c) MB + CuO nanoparticles

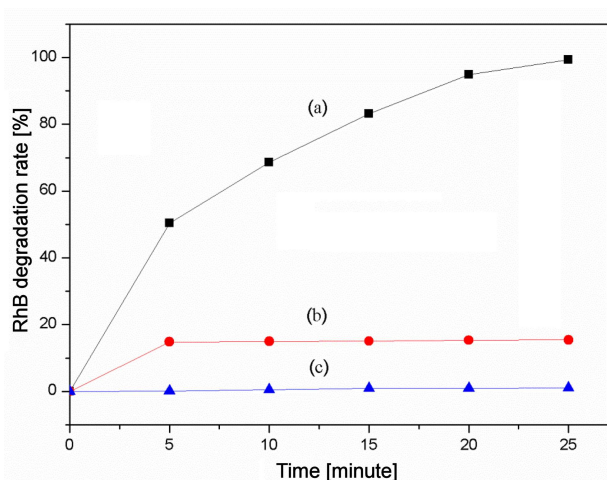


Figure 6. Time profiles of RhB degradation rate:
a) RhB + H₂O₂ + CuO nanoparticles, b) RhB + H₂O₂
and c) RhB + CuO nanoparticles

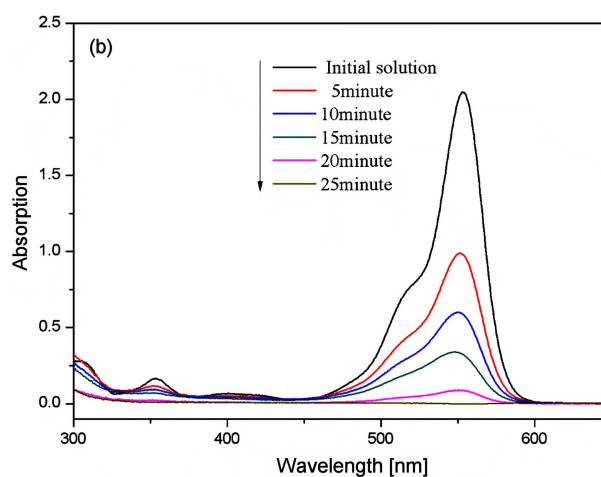
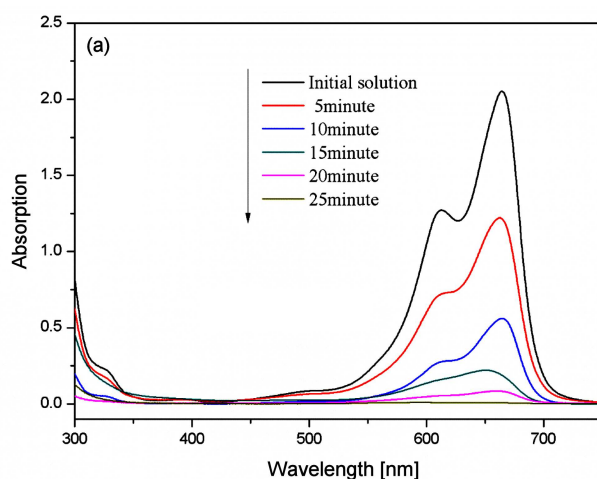


Figure 7. Absorption spectra of methylene blue (a) and rhodamine B (b) solutions in the presence of CuO and H₂O₂ for different time intervals

in the presence of H₂O₂. We obtained the concentration changes of methylene blue and rhodamine B aqueous solutions by means of monitoring methylene blue and rhodamine B absorption at the peak wavelength 664 nm and 554 nm, respectively. As shown in Figs. 5 and 6, after 25 minutes of reaction, the degradation rates with only CuO nanoparticles, for both methylene blue and rhodamine B, are less than 1%. At the same controlling conditions, only in the presence of H₂O₂, the degradation degrees of methylene blue and rhodamine B are both about 15% (Figs. 5 and 6). However, within 25 min of reaction, in the presence of both as-prepared CuO nanoparticles and H₂O₂, the degradation rate of methylene blue and rhodamine B aqueous solutions were 100% and 98% (Figs. 5 and 6), respectively. This demonstrates that the obtained CuO nanoparticles showed good catalytic performance. The corresponding analysis of UV-visible absorption spectra was shown in Fig. 7. The absorption peaks at 664 nm and 554 nm diminished with increasing reaction time, indicating that the rapid degradation of methylene blue and rhodamine B solution was attributed to the decomposition of the dye structure. So far, hydroxyl radicals ($\cdot\text{OH}$) have been suggested to be an effective oxidant for complete oxidising or degrading organic compounds in the aqueous solutions [33–36]. In the catalytic test, the reason of rapid decomposition of methylene blue and rhodamine B is that CuO nanoparticle as the high activity catalyst induced H₂O₂ oxidation to generate free $\cdot\text{OH}$ radical species and ultimately promoted the degradation of rhodamine B and methylene blue molecules. The size of the as-prepared CuO nanoparticles is about 20 nm. Thus, the presence of high catalytic performance for the sample should be ascribed to the nanostructure and accompanying high surface area. The smaller size and larger specific surface area increase the contact area between the catalyst and the H₂O₂ molecules, the more active sites lead to faster reaction rate, which produces $\cdot\text{OH}$ radical species with a higher speed and finally achieves the purpose of rapid degradation [37].

IV. Conclusions

In the present study, CuO nanoparticles were successfully synthesized via ultrasound wave-assisted ball milling at low temperature. The results showed that ultrasound wave is the key factor in facilitating the synthesis of CuO nanoparticles in the process of ball milling. Combining the mechanochemistry and sonochemistry for synthesized of nanoparticles is expected to become a green environmental protection method. In addition, the as-prepared CuO nanoparticles show good catalytic performance for degradation of Methylene blue and Rhodamine B.

Acknowledgements: The author (Ding Chen) greatly acknowledges the financial support by Hunan Provincial Natural Science Foundation of China (14JJ1013).

References

- J. Zhang, A. Yu, "Nanostructured transition metal oxides as advanced anodes for lithium-ion batteries", *Sci. Bull.*, **60** (2015) 823–838.
- D. Chen, H.Y. Liu, S.R. Xia, "One-step decomposition of basic carbonates into single-phase crystalline metallic oxides nanoparticle by ultrasonic wave-assisted ball milling technology", *Ceram. Int.*, **38** (2012) 821–825
- P.R. Solanki, A. Kaushik, V.V. Agrawal, B.D. Malhotra, "Nanostructured metal oxide-based biosensors", *NPG Asia. Mater.*, **3** (2011) 17–24.
- X. Wang, J. Yang, L. Shi, M. Gao, "Surfactant-free synthesis of CuO with controllable morphologies and enhanced photocatalytic property", *Nano. Res. Lett.*, **11** (2016) 125–131.
- W. Yu, J.H. Zhao, M.Z. Wang, Y.H. Hu, L.F. Chen, H.Q. Xie, "Thermal conductivity enhancement in thermal grease containing different CuO structures", *Nano. Res. Lett.*, **10** (2015) 113–120.
- J. Wang, Q. Zhang, X. Li, D. Xu, Z. Wang, H. Guo, K. Zhang, "Three-dimensional hierarchical Co₃O₄/CuO nanowire heterostructure arrays on nickel foam for high-performance lithium ion batteries", *Nano. Energy*, **6** (2014) 19–26.
- L.B. Chen, N. Lu, C.M. Xu, H.C. Yu, T.H. Wang, "Electrochemical performance of polycrystalline CuO nanowires as anode material for Li ion batteries", *Electrochim. Acta.*, **54** (2009) 4198–4201.
- L.B. Luo, X.H. Wang, C. Xie, Z.J. Li, R. Lu, X.B. Yang, J. Lu, "One-dimensional CuO nanowire: synthesis, electrical, and optoelectronic devices application", *Nano. Res. Lett.*, **9** (2014) 637–644.
- S. Sun, X. Zhang, Y. Sun, J. Zhang, S. Yang, X. Song, Z. Yang, "A facile strategy for the synthesis of hierarchical CuO nanourchins and their application as non-enzymatic glucose sensors", *RSC Advances*, **3** (2013) 13712–13719.
- X. Liu, J. Zhang, Y. Kang, S. Wu, S. Wang, "Brochantite tabular microspindles and their conversion to worm-like CuO structures for gas sensing", *Cryst. Eng. Comm.*, **14** (2012) 620–625.
- Y.Z. Feng, X.L. Zheng, "Plasma-enhanced catalytic CuO nanowires for CO oxidation", *Nano. Lett.*, **10** (2011) 4762–4766.
- E. Malka, L. Perelshtein, A. Lipovsky, Y. Shalom, L. Narshekar, N. Perkas, "Eradication of multi-drug resistant bacteria by a novel Zn-doped CuO nanocomposite", *Small*, **9** (2013) 4069–4076.
- J. Ziolo, F. Borsa, M. Corti, A. Rigamonti, F. Parmigiani, "Cu nuclear quadrupole resonance and magnetic phase transition in CuO", *J. Appl. Phys.*, **67** (1990) 5864–5866.
- P. Poizot, S. Laruelle, S. Grugeon, L. Dupont, J-M. Tarascon, "Nano-sized transition-metal oxides as negative-electrode materials for lithium-ion batteries", *Nature*, **407** (2000) 496–499.
- R.V. Kumar, Y. Diamant, A. Gedanken, "Sonochemical synthesis and characterization of nanometer-size transition metal oxides from metal acetates", *Chem. Mater.*, **12** (2000) 2301–2305.
- D. Reznik, L. Pintschovius, M. Ito, S. Iikubo, M. Sato, H. Goka, M. Fujita, K. Yamada, "Electron-phonon coupling reflecting dynamic charge inhomogeneity in copper oxide superconductors", *Nature*, **440** (2006) 1170–1173.
- A. Samad, M. Furukawa, H. Katsumata, T. Suzuki, S. Kaneco, "Photocatalytic oxidation and simultaneous removal of arsenite with CuO/ZnO photocatalyst", *J. Photochem. Photobiol. A: Chem.*, **325** (2016) 97–103.
- P. Deka, R.C. Deka, P. Bharali, "Porous CuO nanostructure as a reusable catalyst for oxidative degradation of organic water pollutants", *New J. Chem.*, **40** (2016) 348–357.
- S. Sonia, S. Poongodi, P.S. Kumar, D. Mangalaraj, N. Ponpandian, C. Viswanathan, "Hydrothermal synthesis of highly stable CuO nanostructures for efficient photocatalytic degradation of organic dyes", *Mater. Sci. Semicond. Process.*, **30** (2015) 585–591.
- S. Zaman, A. Zainelabdin, G. Amin, O. Nur, M. Willander, "Efficient catalytic effect of CuO nanostructures on the degradation of organic dyes", *J. Phys. Chem. Solids*, **73** (2012) 1320–1325.
- M.U. Prathap, B. Kaur, R. Srivastava, "Hydrothermal synthesis of CuO micro-/nanostructures and their applications in the oxidative degradation of methylene blue and non-enzymatic sensing of glucose/H₂O₂", *Colloid Interface Sci.*, **370** (2012) 144–154.
- Y. Yu, J. Zhang, "Solution-phase synthesis of rose-like CuO", *Mater. Lett.*, **63** (2009) 1840–1843.
- Z. Zhang, J. Hao, W. Yang, B. Lu, X. Ke, B. Zhang, J. Tang, "Porous Co₃O₄ nanorods-reduced graphene oxide with intrinsic peroxidase-like activity and catalysis in the degradation of methylene blue", *ACS Appl. Mater. Interfaces*, **5** (2013) 3809–3815.
- P. Deka, R.C. Deka, P. Bharali, "In situ generated copper nanoparticle catalyzed reduction of 4-nitrophenol", *New J. Chem.*, **38** (2014) 1789–1793.
- A.P. Moura, L.S. Cavalcante, J.C. Sczancoski, D.G. Stroppa, E.C. Paris, A.J. Ramirez, J.A. Varela, E. Longo, "Structure and growth mechanism of CuO plates obtained by microwave-hydrothermal without surfactants", *Adv. Powder Technol.*, **21** (2010) 197–202.
- J. Liu, D. Xue, "Thermal oxidation strategy towards porous metal oxide hollow architectures", *Adv. Mater.*, **20** (2008) 2622–2627.
- Z. Yuan, Z.H. Chen, D. Chen, Z.T. Kang, "Analyses of factors affecting nickel ferrite nanoparticles synthesis in ultrasound-assisted aqueous solution ball milling", *Ultrason. Sonochem.*, **22** (2015) 188–197.
- D. Chen, D.Y. Li, Y.Z. Zhang, Z.T. Kang, "Preparation of magnesium ferrite nanoparticles by ultrasonic

- wave-assisted aqueous solution ball milling”, *Ultrason. Sonochem.*, **20** (2013) 1337–1340.
29. D. Chen, H.Y. Liu, “One-step synthesis of nickel ferrite nanoparticles by ultrasonic wave-assisted ball milling technology”, *Mater. Lett.*, **72** (2012) 95–97.
 30. K.S. Suslick, “Sonochemistry”, *Science*, **247** (1990) 1439–1446.
 31. K.S. Suslick, “The chemical effects of ultrasound”, *Sci. Am.*, **260** (1989) 60–62.
 32. R. Feng, Y. Zhao, C. Zhu, T.J. Mason, “Enhancement of ultrasonic cavitation yield by multi-frequency sonication”, *Ultrason. Sonochem.*, **9** (2002) 231–236.
 33. N. Yuan, G. Zhang, S. Guo, Z. Wan, “Enhanced ultrasound-assisted degradation of methyl orange and metronidazole by rectorite-supported nanoscale zero-valent iron”, *Ultrason. Sonochem.*, **28** (2016) 62–68.
 34. L.J. Xu, J.L. Wang, “Magnetic nanoscaled Fe₃O₄/CeO₂ composite as an efficient Fenton-like heterogeneous catalyst for degradation of 4-chlorophenol”, *Environ. Sci. Technol.*, **46** (2012) 10145–10153.
 35. K.M. Thompson, W.P. Griffith, M. Spiro, “Mechanism of peroxide bleaching at high pH”, *J. Chem. Soc. Chem. Commun.*, **21** (1992) 1600–1601.
 36. K.M. Thompson, W.P. Griffith, M. Spiro, “Mechanism of bleaching by peroxides. Part 3. - Kinetics of the bleaching of phenolphthalein by transition-metal salts in high pH peroxide solutions”, *J. Chem. Soc. Faraday Trans.*, **90** (1994) 1105–1114.
 37. W.X. Zhang, Z.H. Yang, X. Wang, Y.C. Zhang, X.G. Wen, S.H. Yang, “Large-scale synthesis of β-MnO₂ nanorods and their rapid and efficient catalytic oxidation of methylene blue dye”, *Catal. Commun.*, **7** (2006) 408–412.